AFRL-RX-WP-TP-2008-4020

MODELLING PLASTICITY OF NI_3Al-BASED $L1_2$ INTERMETALLIC SINGLE CRYSTALS. II. TWO-STEP (T_1 AND T_2) DEFORMATION BEHAVIOUR (POSTPRINT)

Y.S. Choi, D.M. Dimiduk, M.D. Uchic, and T.A. Parthasarathy

UES, Inc.

OCTOBER 2007

Approved for public release; distribution unlimited.

See additional restrictions described on inside pages

STINFO COPY

AIR FORCE RESEARCH LABORATORY
MATERIALS AND MANUFACTURING DIRECTORATE
WRIGHT-PATTERSON AIR FORCE BASE, OH 45433-7750
AIR FORCE MATERIEL COMMAND
UNITED STATES AIR FORCE

REPORT DOCUMENTATION PAGE	Form Approved OMB No. 0704-0188

1. REPORT DATE *(DD-MM-YY)*	2. REPORT TYPE	3. DATES COVERED *(From - To)*
October 2007	Journal Article Postprint	

4. TITLE AND SUBTITLE
MODELLING PLASTICITY OF NI_3Al-BASED $L1_2$ INTERMETALLIC SINGLE CRYSTALS. II. TWO-STEP (T_1 AND T_2) DEFORMATION BEHAVIOUR (POSTPRINT)

5a. CONTRACT NUMBER FA8650-04-D-5233
5b. GRANT NUMBER
5c. PROGRAM ELEMENT NUMBER 62102F
5d. PROJECT NUMBER 2311
5e. TASK NUMBER 00
5f. WORK UNIT NUMBER 23110002

6. AUTHOR(S)
Y.S. Choi and T.A. Parthasarathy (UES, Inc.)
D.M. Dimiduk and M.D. Uchic (AFRL/RXLMD)

7. PERFORMING ORGANIZATION NAME(S) AND ADDRESS(ES)

UES, Inc. 4401 Dayton-Xenia Road Dayton, OH 45432-1894	Metals Branch (AFRL/RXLMD) Ceramics & Nondestructive Evaluation Division Air Force Research Laboratory Materials and Manufacturing Directorate Wright-Patterson Air Force Base, OH 45433-7750 Air Force Materiel Command, United States Air Force

8. PERFORMING ORGANIZATION REPORT NUMBER

9. SPONSORING/MONITORING AGENCY NAME(S) AND ADDRESS(ES)
Air Force Research Laboratory
Materials and Manufacturing Directorate
Wright-Patterson Air Force Base, OH 45433-7750
Air Force Materiel Command
United States Air Force

10. SPONSORING/MONITORING AGENCY ACRONYM(S)
AFRL/RXLMD

11. SPONSORING/MONITORING AGENCY REPORT NUMBER(S)
AFRL-RX-WP-TP-2008-4020

12. DISTRIBUTION/AVAILABILITY STATEMENT
Approved for public release; distribution unlimited.

13. SUPPLEMENTARY NOTES
Journal article published in Philosophical Magazine, Vol. 87, No. 30, 21 October 2007, 4759–4775.

14. ABSTRACT
The two-step (T_1 and T_2) deformation behaviour of Ni_3Al-based single crystals was modelled under the framework of a new constitutive model proposed by Y.S. Choi, D.M. Dimiduk, M.D. Uchic, et al. [Phil. Mag. 87 1939 (2007)]. A new set of formulations and criteria, which identify thermally reversible and irreversible components of the constitutive variable a and define the relative significance of those components, was developed and implemented within the new constitutive framework. The simulation results well captured the general qualitative trends of the flow behaviour upon re-straining at T_2 after pre-straining at T_1 for both $T_1 > T_2$ and $T_1 < T_2$. Modelling results suggested that the dislocation substructures generated at T_1 need to be treated as partially of fully transferable to plastic flow at T_2, at least through the early stage of re-straining, to capture all major pre-strain effects. In particular, the large strengthening effect at T_2 for even a few percent of pre-strain at T_1 was obtainable only by controlling the availability of mobile dislocations and sources at T_2.

15. SUBJECT TERMS
deformation mechanisms, plasticity, intermetallics

16. SECURITY CLASSIFICATION OF: a. REPORT	b. ABSTRACT	c. THIS PAGE	17. LIMITATION OF ABSTRACT:	18. NUMBER OF PAGES	19a. NAME OF RESPONSIBLE PERSON (Monitor)
Unclassified	Unclassified	Unclassified	SAR	24	John Barnes **19b. TELEPHONE NUMBER** *(Include Area Code)* N/A

Standard Form 298 (Rev. 8-98)
Prescribed by ANSI Std. Z39-18

Philosophical Magazine,
Vol. 87, No. 30, 21 October 2007, 4759–4775

Modelling plasticity of Ni_3Al-based $L1_2$ intermetallic single crystals. II. Two-step (T_1 and T_2) deformation behaviour

Y. S. CHOI*‡, D. M. DIMIDUK†, M. D. UCHIC†
and T. A. PARTHASARATHY‡

†Air Force Research Laboratory, AFRL/MLLM, 2230 Tenth Street,
Wright-Patterson AFB, OH 45433-7817, USA
‡UES, Inc, 4401 Dayton-Xenia Rd., Dayton, OH 45432-1894, USA

(*Received 21 February 2007; in final form 6 July 2007*)

The two-step (T_1 and T_2) deformation behaviour of Ni_3Al-based single crystals was modelled under the framework of a new constitutive model proposed by Y.S. Choi, D.M. Dimiduk, M.D. Uchic, *et al*. [Phil. Mag. **87** 1939 (2007)]. A new set of formulations and criteria, which identify thermally reversible and irreversible components of the constitutive variables and define the relative significance of those components, was developed and implemented within the new constitutive framework. The simulation results well captured the general qualitative trends of the flow behaviour upon re-straining at T_2 after pre-straining at T_1 for both $T_1 > T_2$ and $T_1 < T_2$. Modelling results suggested that the dislocation substructures generated at T_1 need to be treated as partially or fully transferable to plastic flow at T_2, at least through the early stage of re-straining, to capture all major pre-strain effects. In particular, the large strengthening effect at T_2 for even a few percent of pre-strain at T_1 was obtainable only by controlling the availability of mobile dislocations and sources at T_2.

1. Introduction

The partially reversible flow stress upon re-straining at T_2 after pre-straining at T_1 ($T_2 \neq T_1$) is one of the key thermomechanical features of Ni_3Al-based intermetallic single crystals. This peculiar behaviour is significant since it holds a clue to understanding the dislocation behaviour, its link to evolving substructures during plastic deformation and how these constituents contribute to the macroscopically-observed flow stress. Since Davies and Stoloff [1] first utilized the two-step (T_1 and T_2) deformation experiment for Ni_3Al to identify the nature of plastic flow, numerous other experimental studies have sought clarification of the mechanisms governing two-step deformation behaviour of $L1_2$ intermetallics [2–13]. Ezz and Hirsch experimentally verified that a Cottrell–Stokes law [14] holds for the deformation structure of $Ni_3(Al,Hf)B$ single crystals, which shows that irreversible dislocation storage processes are partially responsible for strain hardening [15]. However, that same study serves to illustrate the remarkable and exclusively

*Corresponding author. Email: yoon-suk.choi@wpafb.af.mil

Philosophical Magazine
ISSN 1478–6435 print/ISSN 1478–6443 online © 2007 Taylor & Francis
http://www.tandf.co.uk/journals
DOI: 10.1080/14786430701589368

thermally reversible component of the flow stress. This implies that some of the stress-controlling dislocation configurations are thermally reversible, others are irreversible and both may contribute to plastic yielding, sustaining the flow stress and setting the strain-hardening rate (SHR).

Ezz and Hirsch [12] also studied the effect of RT pre-strain ($T_1 \leq T_2$) on the flow-stress anomaly in a $Ni_3(Al,Hf,B)$ single crystal. The study showed that a pre-strain at T_1 significantly changes the temperature dependence of the flow stress, as schematically illustrated in figure 1 (identical to figure 6 in [12]). Here, the temperature dependence of the yield stress for the RT-pre-strained case was divided into two distinct regimes: 'A' ($\mathrm{RT} < T < T_C$) and 'B' ($T > T_C$) by defining a temperature T_C, at which the yield stress ($\tau_{yp}(T)$), upon re-straining at T_2 after pre-straining at RT, is equal to the yield stress ($\tau_y(T)$) without RT pre-straining. In figure 1, regime A exhibits a significantly diminished positive temperature dependence of the yield stress due to RT pre-strain. However, in regime B $\tau_{yp}(T)$ is just slightly lower than $\tau_y(T)$. For compression near the [0 0 1] orientation, T_C was in the range 673–803 K, depending upon the magnitude of RT pre-strain [12].

In contrast to the numerous experimental studies on the two-step deformation behaviour of Ni_3Al alloys [1–13, 15], only a few studies attempt theoretical modelling of this behaviour. Both Ezz and Hirsch [12] and Greenberg and Ivanov [16] proposed theoretical frameworks for the two-step deformation behaviour. However, both of these frameworks were solely qualitative and quantitative modelling has never been attempted.

In [17], the present authors proposed a comprehensive crystallographic constitutive model for Ni_3Al-based intermetallic single crystals. The present study used that constitutive framework to model the two-step deformation behaviour, *viz.* the thermal reversibility of the flow behaviour, of Ni_3Al-based single crystals. Here, both the physical basis for the constitutive model and the understanding gleaned from its framework serve as the conceptual framework for modelling the two-step deformation behaviour. Those concepts are summarized in

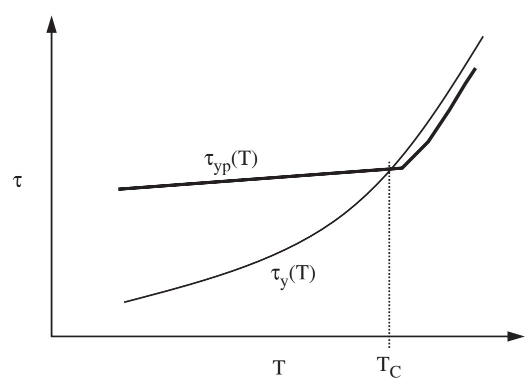

Figure 1. Schematic plot illustrating the effect of RT pre-strain on the positive temperature-dependence of yield stress as adopted from figure 6 in [12]. The plot was based on experimental observations from compression of near-[001]-oriented $Ni_3(Al,1.5\%\ Hf)0.2\%$ B single crystals by Ezz and Hirsch [12].

section 2 of this report. A thorough review of previously published experimental and theoretical work on the two-step deformation behaviour of $L1_2$ single crystals formed the basis for this study (refer to [1–13, 15, 16]). Based upon this review, key concepts for the thermal reversibility of Ni_3Al-based single crystals were identified and used to represent the effect of pre-strain within the framework of our constitutive model. An interpretation of those concepts for the purposes of implementing the present model is discussed in section 3. Finally, numerical simulation was performed to investigate an incorporation of the pre-strain effect in the constitutive model. The results are discussed within the context of their physical implications in sections 4 and 5.

2. Constitutive model proposed in part I

A summary of the new constitutive descriptions for Ni_3Al-based single crystals can be found in section 3.3 of [17]. That constitutive model was structured upon an understanding of the extensive literature describing physically verified micromechanisms associated with the anomalous flow behaviour of Ni_3Al-based $L1_2$ intermetallics. For those materials, upon plastic straining, mobile screw-character superdislocations are 'effectively' instantaneously exhausted by forming Kear–Wilsdorf locks (KWLs) [18, 19]. The locks result from intrinsic elastic and fault-energy related forces, driving cross-slip of screw-character superdislocations from the octahedral plane to the cubic plane, resulting in a range of superlattice-partial dislocation separation distances in the cubic plane. The locking mechanism also results in a spectrum of non-screw-character superdislocation segments, called macrokinks, remaining glissile on the octahedral plane. Thus, elementary glide loops adopt an anisotropic, three-dimensional nature while maintaining effectively octahedral glide. Such exhaustion limits the availability of mobile dislocations, which results in an SHR that well exceeds any rate expected from ordinary FCC single crystals. The exhaustion of mobile dislocations and its influence on the SHR and flow-stress anomaly was theoretically treated by Caillard [20] and numerically modelled by the present authors [21]. The recent slip-trace analysis of Ni_3Al using atomic force microscopy by Fikar *et al.* [22] and Coupeau and Bonneville [23] also confirmed the importance of the mobile-dislocation exhaustion to the SHR and flow-stress anomalies.

The dislocation substructure associated with this exhaustion mechanism is typified by long, straight locked screw-character superdislocations (KWLs) connected by a series of macro-kinks (MKs) and cross-slip jogs (CJs) on the cubic-plane steps connecting the octahedral planes. The new constitutive model represented such dislocation substructures using two important constitutive structure parameters, the critical MK height (h_c) and the average MK height ($\bar{h}$), both determined in the octahedral plane. The parameter h_c is the critical height above which MKs are mobilized and $\bar{h}$ is the average distance that screw-character dislocations glide in the octahedral plane before they are locked. Once mobile screw-character dislocations are 'effectively' immobilised by forming KWLs, further plastic straining is facilitated by two mechanistic events: the mobilization of 'weak'

MKs (edge character) and self (athermal) unlocking of 'weak' KWLs (screw character). The new constitutive model treated the former using a fraction of mobilized MKs (f_{mK}), which is a function of h_c and $\bar{h}$ ($f_{mK} = \exp(-h_c/\bar{h})$) based on the statistical treatment of MK-height populations and the latter using a threshold stress (τ_i), which is the stress required to unlock incomplete KWLs. When the applied stress is not high enough to reach τ_i, *viz*. in the regime dominated by exhaustion of screw-character dislocations, the flow stress and area swept by dislocations is limited primarily by the availability of mobile MKs (f_{mK}) (hence the mobile MK density ρ_{mK}). Here, the average MK height ($\bar{h}$) decreases exponentially with increasing temperature as its magnitude is inversely proportional to the frequency of cross-slip locking, which is a strong positive function of temperature. This means that, in the anomalous temperature domain, one can expect a higher frequency of cross-slip locking with increasing temperature, leading to a decrease in the average value of MK-height, which eventually limits the mobile MK density (ρ_{mK}). Clearly, it is important to accurately represent the MK behaviour in any model that describes the flow stress after pre-straining at different temperatures.

The new constitutive model for Ni_3Al-based single crystals is distinct from conventional constitutive models for fcc crystals. A major difference is the minimal contribution of forest-dislocation obstacles in the new model (at least within the small strain regime). In other words, the area swept by mobile dislocations is primarily limited by 'effectively' trapping screw-character dislocations via KWLs and, thereby, limiting the MK height distribution and mobile density. For this regime, the mobile density is so limited that the stress must rise sharply to maintain an ample supply of dislocations to satisfy the strain rate. Such a mechanism is in stark contrast to what is envisaged for fcc metals, wherein the area swept is limited by dislocations interacting with forest-dislocation obstacles. For the forest-hardening case, the material exhibits a much lower stress sensitivity of the mobile density; thus, there is an abundance of mobile dislocations at comparatively modest stresses.

This KWL-formation, MK-motion mechanism is expected to dominate in the small-strain (up to 3–5% of the axial strain) exhaustion-hardening regime. Thus, in this regime, the flow stress of Ni_3Al may not be quantified through the observed dislocation density and the Taylor-type relationship known to hold for fcc metals. This was indeed the major conclusion drawn by Kruml *et al*. [24] from their measurements of flow stress and the dislocation density for Ni_3Al alloys. The new constitutive model treated these concepts numerically through equations describing the dislocation substructure resulting from such mechanistic processes. Again, the two constitutive parameters, h_c and $\bar{h}$, play key roles in representing the 'strength' and the temperature dependence of such a dislocation substructure. In particular, these two parameters are critical for representing the effect of pre-straining at T_1 (i.e. the influence of the T_1 dislocation substructure on the T_2 deformation) when modelling two-step (T_1 and T_2) deformation behaviour, the details of which are discussed in the next section. Nonetheless, having drawn focus to the primary importance and parameters describing MK behaviour, one cannot ignore fcc-like contributions to strain hardening. Forest-like obstacles pose a resistance to MK glide and contribute to irreversible components of flow stress during two-step deformation sequences, as detailed in what follows.

3. Incorporating the pre-strain effect in the constitutive model

A literature survey [1–13, 15, 16] and interpretation of those reports identified key phenomenological aspects of the two-step deformation behaviour of Ni_3Al-based single crystals; these key points are listed. For the sake of clarity, the word 'original' is used hereafter to refer to the material state that has no pre-strain history.

(i) For $T_1 > T_2$ experiments, the magnitude of pre-strain at T_1 was usually very small, less than about 2.5% shear strain. Even though the flow stress measured when re-straining at T_2 was lower than that for original straining at T_1, the small magnitude of pre-strain at T_1 gave rise to a significant flow-stress increment at T_2. This is expressed by $\Delta\tau = \tau_{(p)} - \tau_{(o)}$, where $\tau_{(p)}$ and $\tau_{(o)}$ are the T_2 flow stresses with and without pre-strain at T_1, respectively. The observed flow-stress increment at T_2, $\Delta\tau$, ranged from 45 to 170% of $\tau_{(o)}$ [5, 6, 9, 13] depending upon the loading orientation, values of T_1 and T_2, the magnitude of pre-strain and the alloy composition. The magnitude of the flow stress determined from strain hardening at T_1 was observed to be comparable to $\Delta\tau$ at T_2. However, from only a few percent pre-strain at T_1 ordinary fcc-like hardening alone is not expected to generate such a large strengthening effect ($\Delta\tau$) at T_2. This implies that strain hardening at T_1 may involve complex dislocation substructures whose strength contributions originate from various sources beyond ordinary fcc-like hardening. Furthermore, these substructure contributions may be partially or fully transferred to the deformation at T_2, hence raising the magnitude of $\Delta\tau$.

(ii) For $T_1 < T_2$ experiments, two distinctive regimes were identified. In the case that a difference between T_1 and T_2 ($\Delta T = T_2 - T_1$) is relatively small (i.e. regime A), a pronounced flow-stress increase was found at T_2 from RT pre-strain experiments [12]. This flow-stress increment at T_2 dramatically decreased with increasing ΔT (hence T_2), resulting in a diminished positive-temperature dependence of the flow stress at T_2 [12]. In the case of a large ΔT (i.e. regime B), the flow stress at T_2 decreased compared to the original flow stress at T_2 by 10–40%, thus initiating a micro-yield transition typically of a magnitude less than a few percent in the small strain regime [5, 13]. These behaviours are sensitive to the magnitude of pre-strain, the loading orientation, ΔT and the alloy composition.

(iii) For both $T_1 > T_2$ and $T_1 < T_2$, the strain-hardening rate of material re-strained at T_2 tended to follow the original flow behaviour at T_2. This trend was more evident for the case of $T_1 > T_2$, wherein crystals exhibited almost identical strain-hardening rates at T_2, with and without pre-strain, after an early substructure-rearrangement stage [6, 9, 13]. However, such a trend was also clear for the case of $T_1 < T_2$, wherein strain-hardening rates for crystals re-strained at T_2 tended to quickly recover the original strain–hardening rate at T_2 after a short re-adjustment (*i.e.* the micro-yield transition) at the early stage of re-straining at T_2 [5, 13]. In this sense, the overall plastic flow of Ni_3Al-based single crystals can be described as a thermally reversible process, the degree of which depends upon the balance between the strengths of reversible and irreversible contributions to plastic flow.

The new constitutive model for Ni_3Al-based single crystals was structured from equation (3) in [17], which can be re-written as:

$$\dot{\gamma} = \dot{\gamma}_K + \dot{\gamma}_w = b\rho_{mK}v_K + b\rho_{mw}v_w. \tag{1}$$

One can refer to [17] for detailed descriptions of each parameter. In equation (1), $\dot{\gamma}_w$ reflects the plastic flow sustained by screw-character dislocations typified by cross-slip locking and athermal unlocking of KWLs having a variable cross-slip distance in the cubic plane, w. This component of the strain rate (stress) can be understood as thermally reversible flow since its basic nature is set by intrinsic driving forces and the '*effectively*' instantaneous rate of KWL formation. The locking rate sets $\dot{\gamma}_w$ and it reflects the present temperature in a fully reversible fashion. This implicitly means that, in equation (1), $\dot{\gamma}_K$ is the term influenced by pre-strain history at T_1 under two-step (T_1 and T_2) deformation. Thus, the plastic strain rate upon re-straining at T_2 after pre-straining at T_1 can be expressed by:

$$\dot{\gamma}_{(p)} = \dot{\gamma}_{K(p)} + \dot{\gamma}_{w(p)} = b\rho_{mK(p)}v_{K(p)} + \dot{\gamma}_w, \tag{2}$$

where all parameters having subscript (p) are in a state at T_2 after being influenced by pre-straining at T_1. Parameters having no subscript (p) are in their characteristic state for T_2 regardless of pre-strain history at T_1. Thus, in equation (2), the influence of pre-strain on plastic flow at T_2 is reflected through $\rho_{\mathrm{mK}(p)}$ and $v_{K(p)}$.

Based upon the viewpoint represented by equation (2) and point (i) at the start of this section, we envisaged that two types of substructures (forest obstacles and MK distributions), which were generated and responsible for strain hardening at T_1, affect plastic flow at T_2. The first, 'forest' obstacles developed and stored at T_1, poses a resistance against the MK glide. That glide resistance was treated through τ_f (equation (17) in [17]), based upon a re-interpretation and simplification of the concept of flow-stress partitioning proposed by Ezz and Hirsch [12, 15, 25]. This irreversible fcc-like obstacle storage was expressed as $\tau_f(T_1, \gamma_1)$, where γ_1 is the shear pre-strain at T_1 and it is assumed to play the same role as obstacles against the MK glide at T_2. Following this assumption, $v_{K(p)}$ in equation (2) can be expressed by:

$$v_{K(p)} = \frac{\tau_{(p)} - \tau_{K(p)}}{B} b, \tag{3}$$

And

$$\tau_{K(p)} = \tau_o + \tau_{f(p)}, \tag{4}$$

$$\tau_{f(p)} = \tau_f(T_1, \gamma_1) + \tau_f, \tag{5}$$

where B is the drag coefficient, and $\tau_{(p)}$ and τ_o are the RSS at T_2 and the CRSS on the octahedral plane, respectively. In equation (4), τ_K is the slip resistance against the MK glide. The evolution of τ_f at T_2 in equation (5) was set to follow a fcc-like parabolic-hardening law as described in equation (18) in [17].

The second substructure type affecting the flow behaviour at T_2 is the MK height configurations, which were generated at T_1. In the new constitutive model [17], plastic flow was controlled by a limited availability of mobile dislocations from both screw-character dislocations being '*effectively*' instantaneously exhausted into KWLs and edge-character dislocations having a mobility controlled by an available MK fraction (see section 3.3 in [17] for details).

Here, the former, namely the formation of KWLs, was treated exclusively as a thermally reversible event through equations (1) and (2) and the associated equations given in [17]. However, the dislocation substructure associated with the MK-height configurations may partially or fully remain after pre-straining at T_1 and probably influences plastic flow at T_2. In other words, the development of new MK-height configurations at T_2 may be influenced by the built-in substructures associated with MK-height configurations at T_1 and γ_1. Also, viewpoint (iii) stated above suggests that such influence of the built-in substructure may be temporary, ranging from the onset of plastic flow until the newly-generated substructure at T_2 gains full control of plastic flow over the old substructure. All of these effects were incorporated into the current model through $\rho_{\mathrm{mK}(p)}$ in equation (2). From equations (5) and (6) in [17], $\rho_{\mathrm{mK}(p)}$ can be expressed as

$$\rho_{mK(p)} = \rho_{Ktot} \exp\left(-\frac{h_{c(p)}}{\bar{h}_{(p)}}\right), \tag{6}$$

where ρ_{Ktot} is the total MK density. As mentioned in the previous section, in the new constitutive model [17], the dislocation substructure associated with MK-height configurations was represented by two key parameters, h_c and $\bar{h}$. In equation (6), these two parameters were used as carriers of substructure between T_1 and T_2 to account for the effect of built-in MK-height configurations at T_1. In the new constitutive model, both h_c and $\bar{h}$ were assumed to asymptotically decay with plastic strain, as expressed by equations (7) and (8) in [17]. Similarly, the evolution of $h_{c(p)}$ and $\bar{h}_{(p)}$ in equation (6) were expressed by:

$$\frac{\mathrm{d}h_{c(p)}}{\mathrm{d}\gamma} = -\theta_{hc(p)}\left(\frac{h_{c(p)} - h_{cs}}{h_{co(p)} - h_{cs}}\right) \tag{7}$$

and

$$\frac{\mathrm{d}\bar{h}_{(p)}}{\mathrm{d}\gamma} = -\theta_{\bar{h}(p)}\left(\frac{\bar{h}_{(p)} - \bar{h}_s}{\bar{h}_{o(p)} - \bar{h}_s}\right), \tag{8}$$

where $\theta_{\mathrm{hc}(p)}$ and $\theta_{\bar{h}(p)}$ are initial decay rates for $h_{c(p)}$ and $\bar{h}_{(p)}$, respectively, and h_{cs} and $\bar{h}_s$ are the final saturation values. From equations (6) through (8), one needs to implicitly understand that the influence of built-in MK-height configurations was incorporated in modelling through the adjustment of initial values of critical and average MK heights ($h_{co(p)}$ and $\bar{h}_{o(p)}$, respectively), and their evolution ($\theta_{\mathrm{hc}(p)}$ and $\theta_{\bar{h}(p)}$) with strain at T_2. The exact arithmetic forms (equations (7) and (8)) representing a smooth evolution of substructure between states T_1 and T_2 are a constitutive assumption. The assumption was chosen because it offers a reasonably well-behaved representation of the understood MK phenomenology within the constitutive model, even though this aspect of MK behaviour has never been quantified.

Figure 2 schematically illustrated these parameters at T_2 for the cases with and without pre-strain at T_1. Figure 2 takes the evolution of h_c at T_2 as an example. Note, however, that the same illustration is also applicable to the evolution of $\bar{h}$ at T_2. Due to pre-strain at T_1, the initial critical MK height at T_2 was assumed to decrease to

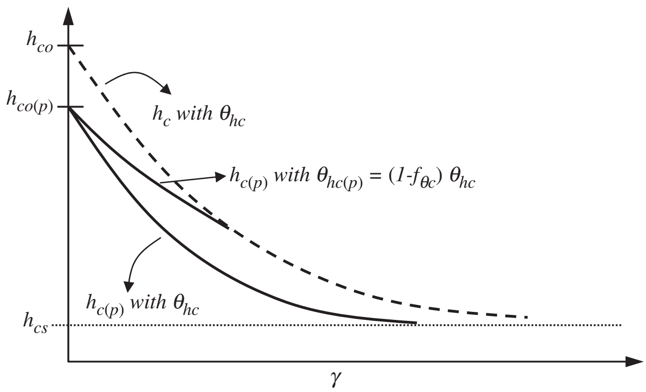

Figure 2. Schematic plot showing the evolution of h_c at T_2 for cases with (two solid lines) and without (broken line) pre-strain at T_1. Dark solid lines indicate $h_{c(p)}$ evolution with different initial decay rates, θ_{hc} and $\theta_{\mathrm{hc}(p)}$, respectively.

$h_{co(p)}$ from h_{co}. In the same way, the initial average MK height at T_2 is expected to decrease to $\bar{h}_{o(p)}$ from $\bar{h}_o$. The values of $h_{co(p)}$ and $\bar{h}_{o(p)}$ depend upon those of $h_c(T_1, \gamma_1)$ and $\bar{h}(T_1,\gamma_1)$, which are the critical and average MK heights, respectively, at the end of pre-straining at T_1. Here, to determine $h_{co(p)}$ and $\bar{h}_{o(p)}$, two preliminary parameters H_{co} and $\bar{H}_o$ were defined by:

and
$$H_{co} = h_c(T_1,\gamma_1) + f_{hc}[h_{co}(T_1) - h_c(T_1,\gamma_1)] \tag{9}$$

$$\bar{H}_o = \bar{h}(T_1,\gamma_1) + f_{ha}[\bar{h}_o - \bar{h}(T_1,\gamma_1)], \tag{10}$$

where f_{hc} and f_{ha} are the adjustable parameters having a range from 1 to 0, determining the relative degree of influence of the MK-height related built-in substructure at T_1 on the development of the MK-height substructure at T_2. They represent the potency of the unknown physical effects of partially relaxing the T_1 substructure on unloading and of transitioning to a new substructure upon straining at T_2. The highest degree of influence is expected for the values f_{hc} and f_{ha} equal to 0. Through equations (6)–(10), the present modelling adopted the concept of viewpoint (iii), which accounts for the pre-strain effect being a temporary effect only in the early stage of plastic flow at T_2. This can be incorporated in modelling by letting $h_{c(p)}$ and $\bar{h}_{(p)}$ follow the same strain evolution as that of h_c and $\bar{h}$, respectively, after the initial re-adjustment stage of plastic flow at T_2. For this, the initial decay rates $\theta_{\mathrm{hc}(p)}$ and $\theta_{\bar{h}(p)}$ for $h_{c(p)}$ and $\bar{h}_{(p)}$ are required to decrease to values lower than θ_{hc} and $\theta_{\bar{h}}$, respectively, when $h_{co(p)}$ and $\bar{h}_{o(p)}$ are lower than h_{co} and $\bar{h}_o$, respectively. This was schematically illustrated in figure 2 by a dark solid line showing the evolution of $h_{c(p)}$ having $\theta_{\mathrm{hc}(p)}$ lower than θ_{hc}.

For the determination of $h_{co(p)}$ and $\bar{h}_{o(p)}$ and their corresponding initial decay rates at T_2 the following equations and criteria were used:

$$\begin{aligned} &h_{co(p)} = H_{co} \quad \text{and} \quad \theta_{hc(p)} = (1 - f_{\theta c})\theta_{hc}, \quad \text{if } H_{co} < h_{co} \\ &h_{co(p)} = h_{co} \quad \text{and} \quad \theta_{hc(p)} = \theta_{hc}, \quad \text{otherwise} \end{aligned} \tag{11}$$

and

$$\begin{aligned} &\bar{h}_{o(p)} = \bar{H}_o \quad \text{and} \quad \theta_{\bar{h}(p)} = (1 - f_{\theta a})\theta_{\bar{h}}, \quad \text{if } \bar{H}_o < \bar{h}_o \\ &\bar{h}_{o(p)} = \bar{h}_o \quad \text{and} \quad \theta_{\bar{h}(p)} = \theta_{\bar{h}}, \quad \text{otherwise.} \end{aligned} \tag{12}$$

Here, h_{co} and $\bar{h}_o$ are the original critical and average MK heights, respectively, at the onset of plastic flow at T_2. These were defined by equations (9) and (11), respectively, in [17]. In equations (11) and (12), $f_{\theta c}$ and $f_{\theta a}$ are another set of adjustable parameters ranging from 0 to 1, depending on the differences between h_{co} and $h_{co(p)}$ ($\Delta h_{co} = h_{co} - h_{co(p)}$) and between $\bar{h}_o$ and $\bar{h}_{o(p)}$ ($\Delta\bar{h}_o = \bar{h}_o - \bar{h}_{o(p)}$), respectively. In general, as Δh_{co} and $\Delta\bar{h}_o$ increase, the corresponding $f_{\theta c}$ and $f_{\theta a}$ are expected to increase to ensure a short re-adjustment period in the early stage of plastic flow at T_2. Note that equations (11) and (12) are effective only when H_{co} and $\bar{H}_o$ are smaller than h_{co} and $\bar{h}_o$, respectively, since otherwise the original h_{co} and $\bar{h}_o$ already take full control of plastic flow even at the initial stage of re-straining at T_2. From equations (9) through (12), one should notice that f_{hc} and f_{ha} control the degree of thermal irreversibility, while $f_{\theta c}$ and $f_{\theta a}$ control the duration of the influence of the built-in T_1 substructure at T_2. The values of f_{hc} and f_{ha} being close to 1 bias flow towards the reversible nature of the substructure associated with MK-height configurations and vice versa.

4. Simulation outline

The two-step (T_1 and T_2) deformation behaviour of Ni_3Al-based single crystals was simulated using the formulations described in the previous section. These formulations were incorporated into the framework of the new constitutive model proposed in [17], and T_1 and T_2 compression simulations were performed for [$\bar{1}$ 2 3]-oriented Ni_3(Al,0.25% Hf) single crystals in an anomalous temperature regime from 300 to 900 K. For the case of $T_1 > T_2$, the [$\bar{1}$ 2 3] compression was simulated up to 1% axial pre-strain at 773 K and the subsequent re-straining simulation was performed at 300 K. For the case of $T_1 \leq T_2$, however, the [$\bar{1}$ 2 3]-compression simulation was performed up to the axial pre-strain levels of 5 and 10% at 300 K and the subsequent re-straining simulations were carried out at temperatures from 300 to 900 K. All simulations were preformed at a strain rate of 5×10^{-5}/s. In the present study, four new variable parameters were introduced in the previous section, f_{hc}, f_{ha}, $f_{\theta c}$ and $f_{\theta a}$, and used for parametric studies. The values of all other input parameters were the same as those used in [17] (see tables 1 and 2 in [17] for details). A preliminary parametric study showed that $f_{\theta a}$ expressed as an asymptotic function of $\Delta\bar{h}_o$ ($f_{\theta a} = 0.5[\Delta\bar{h}_o/20(\text{Å})]^{2/3}$) delivered a reasonable qualitative dependence of $f_{\theta a}$ on $\Delta\bar{h}_o$ with varying T_2 for the simulations of $T_1 < T_2$. Note that the same numerical framework for the two-step (T_1 and T_2) deformation (equations (2)–(12)) was used for both cases of $T_1 > T_2$ and $T_1 < T_2$. The simulation results are discussed based upon qualitative comparisons with the experimental data and the physical metallurgical implications of those results were interpreted in the context of previous anomalous flow theories.

5. Simulation results and discussion

The case of $T_1 > T_2$

Figure 3 shows the simulated [$\bar{1}$ 2 3]-compressive flow curves, which represent re-straining at 300 K after being pre-strained by 1% axial strain at 773 K, for different values of $f_{\rm ha}$ from 0.1 to 0.4. The original flow curves simulated at 300 and 773 K are also shown in figure 3 for comparison. Values of $f_{\rm hc}$, $f_{\theta c}$ and $f_{\theta a}$ were set to 0, 0.1 and 0.5, respectively, for the current simulations. Flow curves simulated for re-straining at 300 K well represented the general trend of the partially reversible flow for this class of alloys [5, 9, 13]. The magnitude of $\tau_f(T_1, \gamma_1)$ (equation (5)) obtained from a 1% axial pre-strain at 773 K was just a few MPa, which was insufficient for obtaining a large flow stress increment ($\Delta\tau = \tau_{(p)} - \tau_{(o)}$) at 300 K, as was experimentally observed. The data from Shi, *et al.* [13], revealed an almost 100% increase of the flow stress for experimental tests similar to these simulations. In the present simulations, such a large value of $\Delta\tau$ turned out to be achievable only by controlling the influence of built-in T_1 substructures, specifically, through decreasing the magnitude of $f_{\rm ha}$ in equation (10). The low magnitude of $f_{\rm ha}$ serves to enhance the reduction of the average MK height ($\bar{h}_{(p)}$) at T_2 (due to pre-straining at T_1), which ends in a decrease of available mobile MK density ($\rho_{{\rm mK}(p)}$) at T_2 (through equation (6)). By changing the value of $f_{\rm ha}$ to 0.4, 0.3 and 0.2 in turn, $\Delta\tau$ was increased to approximately 48, 77 and 130% of the original flow stress at 300 K, respectively. These simulations strongly suggest that a large $\Delta\tau$ for the case of $T_1 > T_2$ arises mainly from the reduced availability of mobile

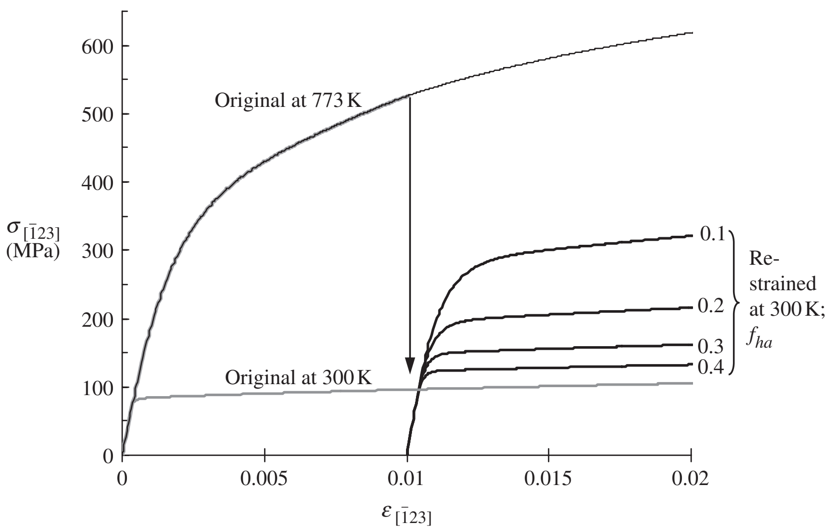

Figure 3. Simulated axial stress *vs.* axial strain curves for different values of $f_{\rm ha}$ from 0 to 0.4 re-strained at 300 K after being pre-strained by 1% axial strain at 773 K. Values of $f_{\rm hc}$, $f_{\theta c}$ and $f_{\theta a}$ were set to 0, 0.1 and 0.5, respectively, for the current simulations. Original axial stress *vs.* axial strain curves simulated at 773 and 300 K, respectively, are also shown for comparison.

dislocations at T_2. Qualitatively speaking, the mobile dislocation density in the early stage of plastic flow is reduced by the influence of the relatively 'strong' MK-height configurations that were built during pre-straining at T_1. This effect was treated by $\rho_{\mathrm{mK}(p)}$ of equation (6) through $h_{c(p)}$ and $\bar{h}_{(p)}$ (equations (7) and (8)) in the current framework of modelling. The simulation results also partly agree with the idea proposed by Shi *et al.* [13], wherein they postulated that a significant reduction of dislocation sources occurs at T_2 as the result of higher temperature pre-straining at T_1.

The case of $T_1 \leq T_2$

Figure 4 shows the simulated 0.2%-offset shear stress ($\tau_{0\cdot2\%}$) *vs.* temperature (T) plots for the cases pre-strained by 5 and 10% at 300 K, followed by re-straining at temperatures from 300 to 900 K (this will be referred to as 'pre-strained' hereafter). Figures 4a and b are the simulation results for two different values of f_{ha}, 0.1 and 0, respectively, where applicable. The simulated original $\tau_{0\cdot2\%}$–T plot (figure 2 in [17]) was also included for comparison. Here, values of f_{hc} and $f_{\theta c}$ were chosen to be 0.2 and 0.4, respectively, for the case of 5% pre-strain, and 0.45 and 0.5, respectively, for the case of 10% pre-strain, and $f_{\theta a}$ was set to asymptotically vary with $\Delta\bar{h}_o$ using a formulation, $f_{\theta a} = 0.5[\Delta\bar{h}_o/20(\text{Å})]^{2/3}$, where applicable. The simulation result well captured the general trend for the effect of RT pre-strain on the positive temperature dependence of the flow stress (schematically illustrated in figure 1), based upon the experimental work by Ezz and Hirsch [12]. A significantly reduced positive temperature dependence of $\tau_{0\cdot2\%}$ was obtained in simulated $\tau_{0\cdot2\%}$–T plots (figures 4a and b) in the temperature regime below T_c (regime A), where T_c was about 600 and 650 K for the cases of 5 and 10% pre-strain, respectively. The major difference in the simulated $\tau_{0\cdot2\%}$–T plots of figures 4a and b is the almost complete absence of the positive temperature dependence of $\tau_{0\cdot2\%}$ in regime A (particularly for 10% pre-strain) for the case of zero f_{ha} (figure 4b), which maximizes the reduction in average MK height at T_2. From equations (10) and (12), the availability of mobile dislocations at the initial stage of plastic flow at T_2 tends to be more limited by decreasing f_{ha} from 0.1 to 0, and this restricted source effect, along with the diminished temperature dependence of $\bar{h}_{o(p)}$ due to zero f_{ha} (equation (15)), is believed to lead to the almost temperature-independent 0.2% flow stresses in regime A in figure 4b (particularly for 10% pre-strain). Here, it was found that equation (12) played a crucial role in determining the critical temperature T_c: $\bar{H}_o < \bar{h}_o$ (hence $\bar{h}_{o(p)} = \bar{H}_o$) for regime A and $\bar{h}_o < \bar{H}_o$ (hence $\bar{h}_{o(p)} = \bar{h}_o$) for regime B.

These effects can be qualitatively described as follows. In regime A, the influence of the built-in T_1 dislocation substructure is so strong that it remains in the subsequent T_2 re-straining and significantly diminishes the temperature-dependent flow (anomaly) at T_2. For this case, the strength of the stored substructure from T_1 masks the flow anomaly in this regime. Without such a T_1 pre-strain, the flow anomaly would dominate the regime. In regime B, however, T_2 is high enough that the KWL-formation rate is high and exhaustion of mobile density dominates flow; hence, the positive temperature-dependence of flow is recovered. For such a case, the stress-controlling MK distribution (mobile density) is dominated by the

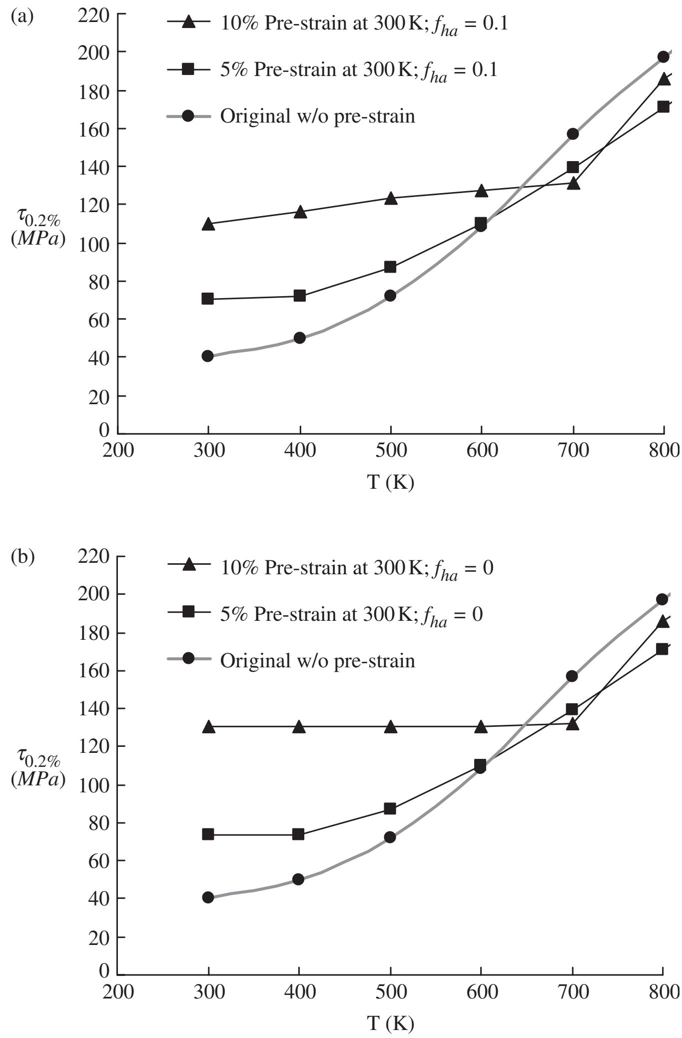

Figure 4. 0.2%-offset shear stress *vs*. temperature plots, simulated for cases pre-strained by 5 or 10% axial strain at 300 K followed by re-straining at temperatures from 300 to 900 K. (a) $f_{ha}=0.1$ and (b) $f_{ha}=0$, where applicable. Values of f_{hc} and $f_{\theta c}$ were set to 0.2 and 0.4 for 5% pre-strain and 0.45 and 0.5 for 10% pre-strain, respectively. The simulated original 0.2%-offset shear stress versus temperature plot is also shown for comparison.

rapid locking of screw-character dislocations at T_2 rather than by the T_1 substructure.

Other comparisons and insights

To gain further insight, the simulated flow curves for selected temperatures in regimes A and B were plotted together. Figure 5 shows simulated 5% pre-strained and original flow curves at 300 and 900 K, which were used to obtain

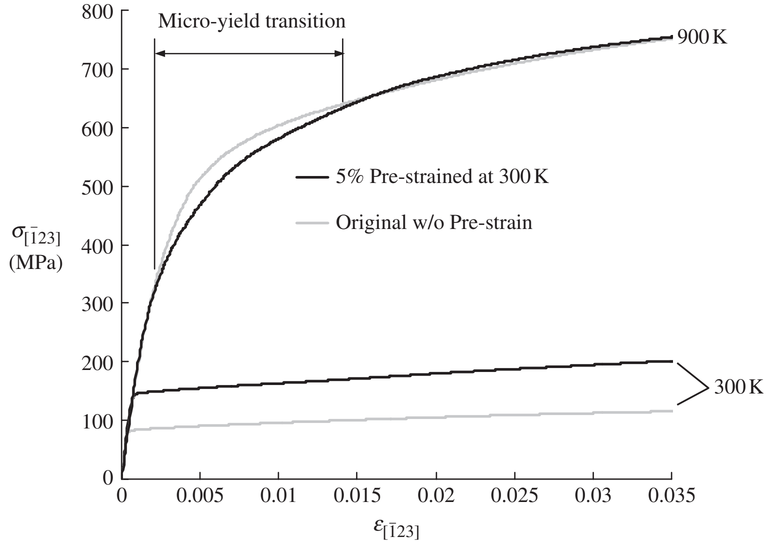

Figure 5. Simulated axial stress *vs.* axial strain curves re-strained at 300 and 900 K, respectively, after being pre-strained by 5% axial strain at 300 K. Values of f_{hc}, $f_{\theta c}$ and f_{ha} were set to 0.2, 0.4 and 0.1, respectively, for the current simulations, where applicable. Original axial stress *vs.* axial strain curves simulated at 300 and 900 K are also shown for comparison.

the $\tau_{0\cdot 2\%}$–T plot in figure 4a ($f_{\mathrm{ha}} = 0.1$). The simulated 5% pre-strained flow curve at 300 K exhibited a monotonic rise over an initial part of the flow curve, with no noticeable change in strain-hardening behaviour when compared to the simulated original flow curves at the same temperature. However, the simulated 5% pre-strained flow curve at 900 K showed a micro-yield transition behaviour in the axial strain range between about 0.3 and 1.4%, as indicated in figure 5. This micro-yield transition seems to be responsible for the slightly decreased pre-strained 0.2% flow stresses, compared to those from original flow curves, in regime B in figure 4a.

As previously mentioned, in regime B, the built-in T_1 substructure effect through $\bar{H}_o$ in equation (10) is no longer expected because $\bar{h}_o < \bar{H}_o$ (hence $\bar{h}_{o(p)} = \bar{h}_o$). However, $H_{co} < h_{co}$ (hence $h_{co(p)} = H_{co}$) still holds, even in this regime. Note that the reduction in the critical MK height ($h_{c(p)}$) due to T_1 pre-strain leads to an increase in mobile MK density ($\rho_{\mathrm{mK}(p)}$) from equation (6). This can be understood as an increased population of mobilized MKs due to the T_1 pre-strain –details of which will be discussed later. Now, initial plastic flow at T_2 tends to rely heavily on the variation of f_{hc} and $f_{\theta c}$ (equations (9) and (11)). In particular, it was discussed in the previous section that the micro-yield transition range at T_2 is controlled by $f_{\theta c}$ (figure 2). Figure 6 shows the simulated 5% pre-strained flow curves at 800 K for two different values of $f_{\theta c}$, 0.4 and 0.6, along with the simulated original flow curve. Initiation of the micro-yield took place at the same axial strain for both 5% pre-strained flow curves having different values of $f_{\theta c}$. However, a more pronounced and extended micro-yield transition was observed as $f_{\theta c}$ decreased from 0.6 to 0.4. Also, upon completion of the micro-yield transition the simulated 5% pre-strained flow

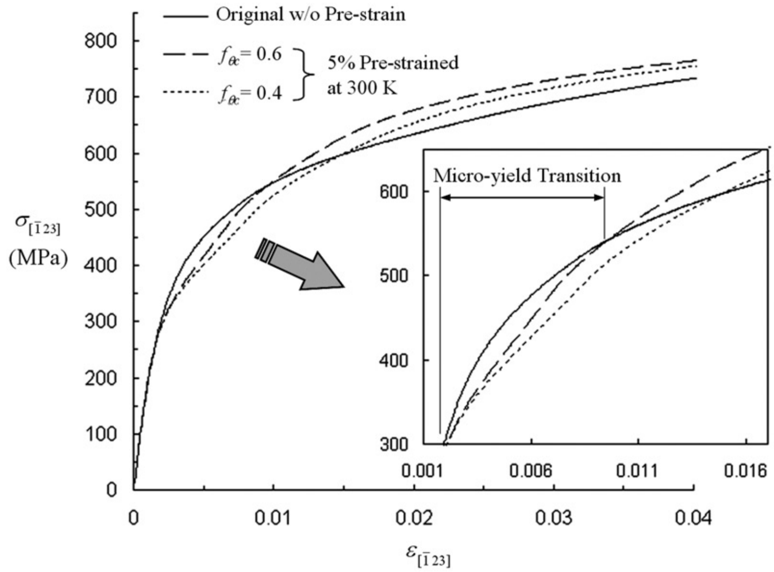

Figure 6. Simulated axial stress *vs*. axial strain curves for two different values of $f_{\theta c}$, 0.4 and 0.6, re-strained at 800 K after being pre-strained by 5% axial strain at 300 K. Values of f_{hc} and f_{ha} were set to 0.2 and 0.1, respectively, for the current simulation. The original axial stress *vs*. axial strain curve simulated at 800 K is also shown for comparison. The insert is the magnified micro-yield transition regime.

curves returned to follow the original strain-hardening behaviour. Note that the micro-yield transition shown in the simulated pre-strained flow curves at 900 K (figure 5) and 800 K (figure 6) is in qualitative agreement with experimental observations for low temperature pre-straining followed by high temperature re-straining [5, 13].

For the case of $T_1 \leq T_2$, the two-step deformation mechanism interpreted from the current simulation results (figures 4–6) was compared to mechanisms proposed by Ezz and Hirsch [12] and Shi *et al.* [13]. In regime A, Ezz and Hirsch [12] ascribed the increased pre-strained flow stresses to the mobile dislocation sources that were already sufficiently hardened during pre-straining at T_1, leading to $\tau_{yp}(T_2)$ larger than $\tau_s(T_2)$ in [12], where $\tau_s(T_2)$ is the athermal bypass stress proposed by Hirsch [26, 27], which was also expressed as a function of $\exp(-H_l/3kT)$ [15], where H_l is the activation energy for cross slip. This is probably in accordance with the built-in T_1 limited-source effect, which was implemented in re-straining at T_2 through the initial average MK height at T_2 ($\bar{h}_{o(p)}$) in equation (12). This occurred because the MK-height configuration (hence the dislocation substructure) introduced by pre-straining at T_1 (represented by $\bar{H}_o$) is stronger than that at T_2 without pre-strain (represented by $\bar{h}_o$), for which in turn $\bar{H}_o < \bar{h}_o$ (hence $\bar{h}_{o(p)} = \bar{H}_o$). In regime B, however, they suggested that $\tau_{yp}(T_2)$ is almost comparable to $\tau_s(T_2)$, which implies that the reversible nature of $\tau_s(T_2)$ dominates the pre-strain effect. In the present simulation, $\bar{h}_{o(p)}$ returns to the original $\bar{h}_o$ in regime B because $\bar{H}_o$ is no longer strong enough to defeat $\bar{h}_o$ in this regime. Hence, $\bar{h}_{o(p)}$ equals $\bar{h}_o$. This means that it takes

back the thermally reversible nature of $\bar{h}_o$ (equation (11) in [17]), which led to the recovered positive temperature dependence of the flow stress in regime B. They also suggested that the slightly decreased $\tau_{yp}(T_2)$, compared to $\tau_y(T_2)$, in regime B was attributed to the propagation of long edge-character dislocations, which was facilitated by forest obstacles inherited from pre-straining at T_1 [12].

Furthermore, Shi *et al*. [13] suggested that the micro-yield transition in the early stage of plastic flow at T_2 was the result of an additional population of large MKs built during pre-straining at T_1. In the present simulation, the micro-yield transition and, hence, the corresponding flow-stress drop in regime B arose because the critical MK height, determined from the T_1 pre-strain (represented by H_{co}), was still smaller than that at T_2 without pre-strain (represented by h_{co}) in this regime; hence $h_{co(p)} = H_{co}$. In other words, some population of larger MKs was carried from T_1 to T_2 through $h_{co(p)}$.

Although there were slight disparities in the detailed understanding of responsible mechanisms, interpretations of pre-straining effects discussed in the literature were in overall agreement with the present simulations. This is particularly true with respect to the idea of a temporary 'readiness' for mobilization and propagation of edge-character dislocations, mainly MKs at the early stage of re-straining at T_2, being responsible for the slight flow-stress drop and the occurrence of the micro-yield transition in regime B. Also note that there is excellent overall accord between the controlling mechanisms deduced from the present modelling and those previously proposed from experimental studies [12, 13]. However, even with such a model and clear evidence of MK-controlled stress, there is no new light to be shed upon the exact mechanisms by which a sufficient population of MKs persists in the substructure, even after saturation of straining under sustained load, as performed by Ezz and Hirsch [15]. One is only left to conclude that some substructure relaxation always takes place on unloading from T_1, leaving mobile segments in the substructure. Upon re-loading at T_2, the stress to activate and multiply dislocations from those segments over a range of strain will be controlled by either the details of the T_1 structure or the KWL-controlled mobile density at T_2, depending upon the values of T_1, T_2, strains at each temperature or their sequence in time.

6. Concluding remarks

We have shown that the two-step (T_1 and T_2) deformation behaviour of Ni_3Al-based single crystals can be qualitatively represented under the framework of a new constitutive model proposed in [17]. Pre-strain at T_1 gave rise to substantial changes of plastic flow at T_2, such as a significant increase in flow stress ($\Delta\tau$), weakened positive temperature-dependence of flow stress and the occurrence of a micro-yield transition. All these pre-strain effects were found to be qualitatively but self-consistently resolved in modelling through a reasonable partitioning of reversible and irreversible contributions of the dislocation substructures, i.e. by understanding the dislocation substructures evolving at T_1 and through controlling the strain duration of these contributions at T_2. In particular, a large flow-stress increment at

T_2, despite only a small magnitude of pre-strain at T_1, was achievable by controlling the availability of mobile dislocations and sources at T_2.

The present constitutive modelling was able to qualitatively capture all such behaviours, since it was able to handle the density of mobile dislocations, in particular, a mobile MK density (ρ_{mK}), as a direct constituent of plastic flow. This approach is significantly distinct from conventional crystallographic constitutive models in which an abundant mobile density is inferred and stress is linked to the Taylor-type homogenization ($\tau_{strength} \sim \alpha\mu\rho^{1/2}$) rule. In those models, the total dislocation density is stress-controlling and evolves according to phenomenological rules for storage and recovery. In the new model, the mobile dislocation density is a degree of freedom itself, which is directly linked to evolution statistics of the MK height distribution and may limit stress, depending on temperature and strain history.

Acknowledgements

This study was supported by the US Defense Advanced Research Projects Agency and the Air Force Office of Scientific Research. YSC and TAP acknowledge support from the Materials and Manufacturing Directorate under the contract # FA8650-04-D-5233. The authors acknowledge fruitful discussion with Dr S. Rao of UES, Inc. and Dr C. Woodward of AFRL/MLLM. The computations described in this study were performed using computer resources at the Ohio Supercomputer Centre (grant #s PAS0647 and PAS0191) with the collaboration of Professor G. Daehn and Professor S. Ghosh of Ohio State University.

References

[1] R.G. Davies and N.S. Stoloff, Trans. Metall. Soc. AIME **233** 714 (1965).
[2] P.H. Thornton, R.G. Davies and T.L. Johnston, Metall. Trans. **1** 207 (1970).
[3] R.A. Mulford and D.P. Pope, Acta Metall. **21** 1375 (1973).
[4] M.H. Yoo and C.T. Liu, J. Mater. Res. **3** 845 (1988).
[5] W.E. Dowling and R. Gibala, In *High-Temperature Ordered Intermetallic Alloys III*, MRS Symp. Proc. Vol. 133, edited by C.C. Kock, C.T. Liu, N.S. Stoloff, *et al.* (MRS, Pittsgurgh, PA, 1989), p. 209.
[6] D.M. Dimiduk and T.A. Parthasarathy, Phil. Mag. Lett. **71** 21 (1995).
[7] D.M. Dimiduk, J. Phys. III **1** 1025 (1991).
[8] S.S. Ezz and P.B. Hirsch, in *High-Temperature Ordered Intermetallic Alloys VI*, MRS Symp. Proc. Vol. 364, edited by J. Horton, I. Baker, S. Hanada, *et al.* (MRS, Pittsgurgh, PA, 1995), p. 35.
[9] K.J. Hemker, M.J. Mills, K.R. Forbes, *et al.*, in *Modeling the Deformation of Crystalline Solids*, edited by T.C. Lowe, A.D. Rollett, P.S. Follansbee, *et al.* (TMS Press, Warrandale, PA, 1991), p. 411.
[10] K.J. Hemker, M.J. Mills and W.D. Nix, J. Mater. Res. **7** 2059 (1992).
[11] A. Couret, Y.Q. Sun and P.B. Hirsch, Phil. Mag. A **67** 29 (1993).

[12] S.S. Ezz and P.B. Hirsch, Phil. Mag. A **73** 1069 (1996).
[13] X. Shi, G. Saada and P. Veyssière, Phil. Mag. A **73** 1419 (1996).
[14] A.H. Cottrell and R.J. Stokes, Proc. R. Soc. Lond. A **233** 17 (1955).
[15] S.S. Ezz and P.B. Hirsch, Phil. Mag. A **69** 105 (1994).
[16] B.A. Greenberg and M.A. Ivanov, Mater. Sci. Eng. A **239/240** 813 (1997).
[17] Y.S. Choi, D.M. Dimiduk, M.D. Uchic, *et al.*, Phil. Mag. **87** 1939 (2007).
[18] B.H. Kear and H.G.F. Wilsdorf, Trans. AIME **224** 382 (1962).
[19] B.H. Kear, Acta Metall. **12** 555 (1964).
[20] D. Caillard, Acta Mater. **44** 2773 (1996).
[21] Y.S. Choi, D.M. Dimiduk, M.D. Uchic, *et al.*, Mater. Sci. Eng. A **400/401** 256 (2005).
[22] J. Fikar, C. Coupeau, T. Kruml, *et al.*, Mater. Sci. Eng. A **387/389** 926 (2004).
[23] C. Coupeau and J. Bonneville, App. Phys. Lett. **90** 171914 (2007).
[24] T. Kruml, J.-L. Martin and V. Paidar, in *Structural Intermetallic* 2001, Proceedings of the 3rd International Symposium on Structural Intermetallics, edited by K.J. Hemker, D.M. Dimiduk, H. Clemens, *et al.*, (TMS Press, Warrendale, PA, 2001), p. 457.
[25] S.S. Ezz and P.B. Hirsch, Phil. Mag. A **72** 383 (1995).
[26] P.B. Hirsch, Phil. Mag. A **65** 569 (1992).
[27] P.B. Hirsch, Prog. Mater. Sci. **36** 63 (1992).